Measurement of local heat flow in flat evacuated glazing

R. E. COLLINS, C. A. DAVIS, C. J. DEY, S. J. ROBINSON, J.-Z. TANG and G. M. TURNER

School of Physics, University of Sydney, Sydney, 2006, Australia

Abstract—A guarded hot-plate apparatus has been developed for measuring the local thermal conductance of flat evacuated glazing. Parasitic heat flows in the apparatus have been reduced to below an equivalent thermal conductance of 0.01 W m^{-2} K^{-1}. Techniques are described for determining the separate contributions to heat flow through the sample from pillar conduction, conduction through residual gas, and radiation. The accuracy of the measurement system is estimated to be better than ±2% and the reproducibility for sequential measurements is better than ±0.004 W m^{-2} K^{-1} for a measurement area of approximately 1.7 cm^2.

1. INTRODUCTION

THE DEWAR flask consists of two concentric cylindrical containers separated by an evacuated space [1]. The vacuum effectively eliminates conductive and convective heat flow from the inner container. Low emittance coatings on the vacuum side of one, or both containers result in very low levels of radiative heat flow. The cylindrical geometry of the Dewar flask is a key feature of the design. This shape is intrinsically strong, since thin-walled containers can withstand the large forces due to atmospheric pressure. In addition, the only mechanical connections between the inner and outer containers occur at the neck of the vessel where they are joined and, in some designs, at a few other points for mechanical stabilisation of the inner container.

It has long been recognized that the insulating principles of the Dewar flask can be applied to flat transparent glazing [2]. Recently, it has been shown [3, 4] that flat evacuated glazing has the potential to achieve an effective thermal conductance below 0.6 W m^{-2} K^{-1}, which is half the best commercially available double glazing, and close to that achieved in windows using multiple glazings and low thermal conductance gas.

A designer of flat evacuated glazing is faced by a fundamental difficulty associated with the effects of atmospheric pressure. A flat structure does not possess the high intrinsic strength of a cylinder when subjected to a large pressure differential. Indeed, virtually all proposals for flat evacuated glazing envisage the necessity for an array of support pillars over the entire evacuated area to maintain the separation of the two glass sheets.

This paper discusses the accurate measurement of heat flow through flat evacuated glazing. This is a much more difficult problem than the characterization of heat flow from a Dewar flask. In the first place, the geometry of a Dewar flask defines a region which is well thermally isolated, and which can be maintained under essentially isothermal conditions. The insulation which is to be characterized surrounds this region. In contrast, in evacuated glazing, the measuring apparatus is external to the structure, and the insulating region (the vacuum) is internal. The measurement apparatus is therefore much more susceptible to heat transport to the surroundings. Secondly, in a Dewar flask, the quantity of interest is the *total* heat flow. In evacuated glazing, total heat flow is also important, particularly if the performance of an entire window in an application is to be characterized. In our measurements, however, we are interested in determining *local* heat transport. In particular, we wish to determine the heat flow through the vacuum space separately from that through the pillars. This requires a measurement of heat flow through an area of order 1 cm^2. The absolute amount of heat flow in this measurement is therefore much smaller than in the case of a Dewar flask.

A third difficulty in characterizing the heat flow through evacuated glazing relates to the structure of the glazing itself. The insulating properties of evacuated glazing arise from the evacuated layer. By definition, this layer is enclosed by two sheets of relatively highly thermally conducting material—the glass plates. The existence of these good thermal conductors can lead to lateral heat flow along the glass sheets, which contributes to the measured value of heat flow in the apparatus. In addition, as discussed below, the presence of a good thermal conductor in contact with the measuring apparatus causes a reduction in sensitivity of the apparatus.

There are important motivations for developing an apparatus which can accurately characterize the local heat flow in evacuated glazing. Evacuated glazings

NOMENCLATURE

A	area of metering piece	ε'	effective emittance of a surface
D	diameter of metering piece	$\varepsilon_{combined}$	combined emittance of two parallel surfaces
L	distance from pillar		
p	gas pressure	σ	Stefan–Boltzmann constant
Q	rate of heat flow	θ	polar angle, measured from normal to surface.
R	resistance of thermistor		
t	thickness of glass plates		
T	temperature		
X	distance between outer edge of guard and inner edge of edge seal	Subscripts	
Z	thermal impedance.	c	cold plate
		h	hot guard
Greek symbols		m	metering piece
$\varepsilon(\theta)$	total directional (angular) emittance of a surface	1, 2	inner surfaces of glass plates.

have the potential for widespread application in low energy buildings. Therefore, it is necessary to demonstrate that the insulating behaviour of the windows is stable over long periods of time. The insulation could degrade because of slight loss of vacuum, or because of an increase in the emittance of the internal coatings. There is a need to undertake extensive ageing studies to investigate such effects. This can only be done non-destructively if the heat flow can be accurately measured. In addition, in order to identify the physical processes which may cause degradation, the contribution to heat transport from the separate physical processes—gas conduction, radiation and pillar conduction—must be identified. A method is discussed for achieving this from accurate local heat transport data.

2. EXPERIMENTAL DESIGN

The aim of the work discussed here is to develop an apparatus which can measure the thermal conductance of evacuated glazing to high reproducibility and accuracy. High reproducibility is an essential requirement in order to undertake an effective life-test program of evacuated glazing. The requirement for high accuracy is imposed in order to enable quantitative estimates to be made of large-area thermal behaviour from small-area measurements. In addition, a high accuracy instrument provides a novel and potentially powerful method of measuring thermal emittance of small area, flat samples. A target resolution for the instrument was set at ± 0.01 W m^{-2} K^{-1} —approximately 2 orders of magnitude less than the design goal for thermal conductance of evacuated glazing.

2.1. Evacuated glazing

A schematic diagram of the transparent evacuated glazing used in this study is shown in Fig. 1, and has

been described in detail elsewhere [3, 4]. Two flat sheets of glass are hermetically sealed around the edges and separated by a square array of support pillars. The space between the sheets is evacuated through a small tube which is subsequently sealed. Heat flow through the structure can occur due to pillar conduction, radiation, and conduction through residual gas. A detailed treatment of these separate effects has appeared elsewhere [3–6]. The design target for the total thermal conductance of evacuated glazing is taken to be 0.6 W m^{-2} K^{-1} with about equal contribution from heat flow through the pillars, and from radiation.

The competing effects of heat flow through the pillars and mechanical tensile stresses in the glass plates lead to a limited range of allowable dimensions for the pillar array. Full details of the design process are presented elsewhere [4–6]. Typical values for the dimensions for short pillars, and 4 mm thick glass
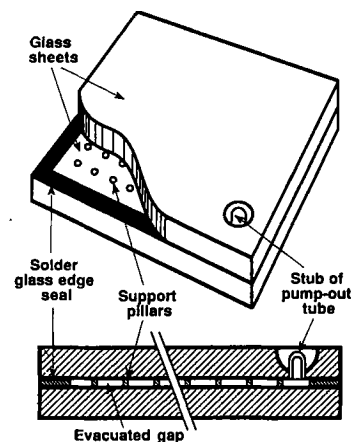

FIG. 1. Schematic diagram of evacuated glazing, showing the square array of pillars between the glass sheets, and the pumpout tube.

are: pillar separation equal to 23 mm and a pillar radius of 0.18 mm.

As will be shown, in practical evaluated glazing with a pillar array as specified above, the heat flow at any point on the surface contains significant contributions from both pillars and radiation. This has important implications for high accuracy measurements such as are required, for example, in a life-test program. The heat flow through the pillars is dependent on the measurement position, so very accurate and reproducible positioning of the apparatus is necessary. It is clearly desirable in such a situation to reduce the contributions from the pillars to small, or negligible levels, over the measurement area. This can only be done by increasing the separation of the pillars and decreasing their size. This increases the tensile stress in the glass plates to levels which are significantly greater than those specified in design standards [7]. Our experience has shown, however, that experimental samples can be constructed and used in the laboratory with larger stress than normally acceptable for field applications. For example, glazing with 4 mm thick glass and a pillar separation of 40 mm seldom develops fractures in the region of external tensile stress above the support pillars. If the pillar separation is increased to 50 mm, however, delayed failures are often observed over periods of 6–12 months. We therefore use a pillar separation of 40 mm in samples designed for thermal stability life tests, but emphasize that the stresses in such samples are unacceptably large for production devices and field applications.

2.2. Principle of the measurement method

A schematic diagram of the apparatus is shown in Fig. 2. The apparatus operates on the principle of the guarded thermal hot plate [8]. A small area thermal conductor, referred to as the 'metering piece' here, is located in good thermal contact with one side of the sample. The metering piece is enclosed by a guard which is also in good thermal contact with the sample, and which is maintained at a constant, 'hot' temperature T_h. In order to maintain the spatial configuration of the metering piece and guard, both components are fixed with epoxy resin to a thin (2 mm) glass plate. A water soluble gel is used to ensure good

thermal contact between this glass plate and the glass of the sample.

The other side of the sample is maintained at a lower, 'cold' temperature, T_c. Due to heat flow through the sample, the temperature of the metering piece, T_m, is less than T_h. A measurement of $T_h - T_m$ therefore provides an estimate of the magnitude of the heat flow. This estimate can be made absolute by dissipating a known amount of thermal power in the metering piece. This increases T_m; when $T_m = T_h$, no heat flow occurs between the metering piece and the guard, and all of the thermal power supplied to the metering piece flows through the sample. In fact, a linear relation exists between $T_h - T_m$ and power, so the null condition $(T_m = T_h)$ can be determined by interpolation.

In order to use this method for precise measurements, several matters must be addressed. It must first be recognized that the metering piece and the guard are in quite good thermal contact since they both touch the relatively high thermal conductance glass of the sample. In fact, the thermal impedance between the metering piece and the guard, Z_{m-h}, is much smaller than that between the metering piece and the cold side, Z_{m-c}, for all samples of practical interest. When no power is dissipated in the metering piece, the temperature difference between the metering piece and the guard due to a given heat flow through the sample, Q, is therefore very small:

$$T_h - T_m = Q \cdot Z_{m-h} \ll T_h - T_c \approx Q \cdot Z_{m-c}. \quad (1)$$

In order to achieve high sensitivity and accuracy, it is thus necessary to measure very small temperature differences. Further, it is essential to establish the existence of the null condition, $T_h = T_m$, to high accuracy. This is particularly important if non-absolute temperature sensors, such as thermistors, are used.

The requirement to measure heat flow to high accuracy imposes an additional constraint: parasitic heat flows from the metering piece to the external surroundings must be reduced to very low values. There are two principal sources of such heat flow: along the wires which provide power and sensing functions to the metering piece; and laterally along the glass plates of the glazing itself. Means of reducing these parasitic heat flows, and other sources of errors, are addressed in detail in the following subsections. Experimental data which demonstrate the level of performance that has been achieved are presented in the Results section.

2.3. Design and construction of the apparatus

In this section, we discuss the factors which determine the critical dimensions of the thermal conductance measuring apparatus and its method of construction. In general, the dimensions are set by the samples to be measured, rather than by some intrinsic feature of the measuring method itself. In order that the design methodology can be applied in other situations, however, some of the results are presented in dimensionless form. A useful scaling parameter is the
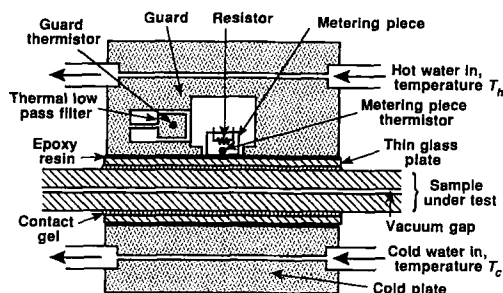

FIG. 2. Schematic diagram of the measuring apparatus.

thickness of the glass on the high temperature side of the apparatus. In this regard, the relevant dimension is the *total* glass thickness—that is the thickness of the glass sheet on the hot side of the sample plus the thickness of the glass sheet to which the metering piece and guard are bonded.

In the following discussion, it is assumed that the metering piece and the guard are both essentially isothermal. Both of these components are machined from brass, the thermal conductivity of which ($110 \ \mathrm{W} \ \mathrm{m}^{-1} \ \mathrm{K}^{-1}$) is more than two orders of magnitude greater than that of glass ($0.78 \ \mathrm{W} \ \mathrm{m}^{-1} \ \mathrm{K}^{-1}$). Consequently, the temperature non-uniformities in these pieces are quite small. Effects due to departures from isothermality are discussed below.

One important feature which determines the sensitivity and accuracy of the apparatus is the area of the metering piece. Ideally, this should be as large as feasible subject to the requirement that it is possible to distinguish between heat flow due to pillars and that due to gas conduction and radiation. The diameter of the metering piece is therefore largely constrained by the dimension of the samples to be measured: in particular by the dimensions of the pillar array and by the thickness of the glass plates. The apparatus was designed with a metering piece of diameter of 12 mm. This provides reasonable spatial resolution for a total glass thickness of 6 mm (4 mm in the sample, and 2 mm in the apparatus) and a pillar separation of 23 mm. As will be shown, it also results in a very small contribution from the pillars to total heat flow at a point mid-way between the pillars for life-test samples with a pillar separation of 40 mm.

A second important factor which determines performance is the thermal impedance between the metering piece and guard, Z_{m-h}. Interestingly, there is little design freedom in this regard. Finite element modelling shows that Z_{m-h} is not a strong function of the annular gap between these two elements. For a 12 mm diameter metering piece, a 2 mm wide annular gap and a total glass thickness of 6 mm, Z_{m-h} changes by only 3.7% for a 10% change in the gap. The choice of gap is therefore determined by factors such as ease of construction and the desirability of defining the effective area for heat flow. Our apparatus has a 2 mm wide gap between the metering piece and the guard. For these dimensions, modelling predicts $Z_{m-h} = 27 \ \mathrm{K} \ \mathrm{W}^{-1}$ for 6 mm thick glass. The measured value in our apparatus is $19 \ \mathrm{K} \ \mathrm{W}^{-1}$.

For high accuracy measurement, it is necessary to know the effective area of the metering piece. The effective area is defined as that area for which the heat flow for zero gap would equal that which occurs in the actual apparatus. Finite element modelling gives the effective area as a circle of radius 6.94 mm—very close to the mid-point of the gap.

The outside diameter of the guard is determined by the requirement that lateral parasitic heat flow from the metering piece along the glass plate should be negligible. Heat can flow along the glass, both to the

surroundings and also, through the edge seal, to the cold side of the sample. In order to verify that such heat flow is negligible in our design, we have modelled a worst case situation—a cylindrically symmetric sample with a bonded edge near the outer diameter of the guard. Figure 3 shows the modelling results for the temperature gradient in the glass, due to lateral heat flow. The gradient is determined at the interface with the guard, in the direction normal to the interface. The guard diameter is 100 mm, and the total glass thickness on the hot side is 6 mm. The temperature gradient decreases approximately exponentially with distance into the guard; the characteristic distance for the gradient to change by a factor of e is approximately 2/3 of the total glass thickness. The heat flow from the metering piece can be obtained by integration. When the bonded edge of the sample is outside the guard region, this heat flow is readily shown to be negligible compared with the target sensitivity of the apparatus of $0.01 \ \mathrm{W} \ \mathrm{m}^{-2} \ \mathrm{K}^{-1}$. The data in Fig. 3 are for the guard temperature equal to the ambient temperature. Modelling shows that operation of the guard above ambient temperature causes only a slight increase in the heat flow from the metering piece. Lateral heat flow along the glass plates is therefore negligible for a 100 mm diameter guard and 6 mm thick glass.

It is important to note the undesirable increase in the heat flow from the metering piece when the bonded edge of the sample is underneath the guard. There is a further reason why this should be avoided: the large heat flow directly through the bonded edge can perturb the temperature of the hot water which defines the temperature of the guard, leading to an inaccurate estimate of the null condition. For precise measurements, it is therefore essential that the entire guard should be located over the evacuated part of the sample, away from the bonded edge. The small
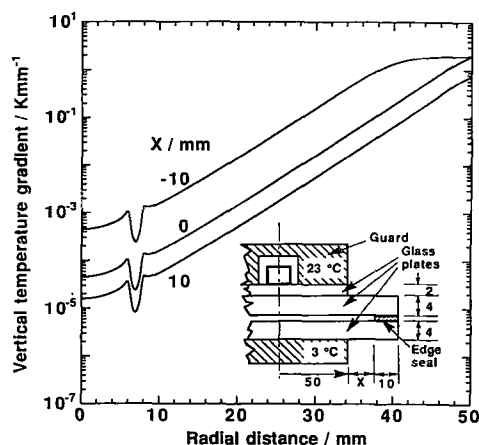

FIG. 3. Temperature gradient in the direction normal to the interface, at the glass side of the interface with the metering piece and guard, for a cylindrically symmetric sample with a bonded edge close to the outer diameter of the guard. A schematic diagram of the apparatus giving the relevant dimensions and temperatures is also shown.

amount of heat flow through the support pillars does not cause a significant change in the temperature of the hot water.

A second source of parasitic heat flow from the metering piece to the surroundings is along the connection wires to the power resistor and temperature sensor. This heat flow can be reduced to negligible levels by using very fine copper connection wires (0.1 mm diameter) and bringing them into good thermal contact with the guard before they are connected to the external circuitry.

As discussed above, the detection to high sensitivity of the null condition, $T_m = T_h$, is of critical importance. Since this is a null method, the main requirements for the temperature sensors are sensitivity and stability. Linearity, whilst a useful feature, is less important. The two sensors considered for this application are thermocouples and thermistors. Thermocouples have the advantage that the condition of temperature equality gives zero output, in principle. They are, however, much less sensitive than thermistors. The use of thermistors necessitates the establishment of the condition $T_m = T_h$ in an independent measurement. In addition, it is necessary to dissipate power in a thermistor in order to measure its resistance.

Following extensive testing with both types of sensors it became clear that the much higher sensitivity of thermistors provides an overwhelming advantage. These devices are therefore used in the apparatus to detect the temperature difference between the metering piece and the guard. Thermistors having a nominal resistance of 220 kΩ at room temperature are used in a bridge configuration with an applied d.c. voltage of 6 V. Although the power dissipation in the metering piece thermistor is greater than the target sensitivity of the apparatus, it remains constant with time and the offset signal that results does not vary during the procedures for establishing the null condition and measuring the heat flow (discussed in the next subsection). The dependence of bridge output on applied bridge voltage is consistent with the measured value of Z_{m-h} and the calculated power dissipation in the metering piece thermistor.

The resistance of the thermistors has the form $R = 0.137 \exp (4200/T)$ ohms, where T is the temperature of the thermistor in Kelvin. The temperature coefficient of the resistance of the thermistors is thus 0.048 K^{-1} at 23°C. Small differences in this coefficient between the guard and metering piece thermistors cause the output of the bridge to change as a result of changes in the temperature of the hot bath, T_h. This effect can be greatly reduced by inclusion of an additional resistor in one of the thermistor arms of the bridge circuit. The value of this resistor is chosen by measuring the temperature dependence of bridge ouput; the resistor typically has a value of a few percent of the thermistor resistance.

A d.c. amplifier is incorporated into the apparatus to reduce electrical noise to negligible levels. The amplifier is based on a Maxim 430CPA high quality

chopper-stabilised operational amplifier. The gain of the amplifier depends on the magnitude of the resistance of the thermistors in the bridge circuit. At 23°C the amplifier gives an output voltage with a gain of five compared with the open circuit bridge voltage. A temperature difference of 1°C between the metering piece and guard therefore corresponds to an output voltage of 0.72 V.

The constant temperatures on the hot and cold sides of the apparatus are maintained with Julabo F20-HC water baths which have a specified temperature stability of ± 0.01°C. The internal pumps of the baths are used to circulate water to each side of the apparatus through well insulated pipes. Flow rates are about 0.05 l s^{-1}. The temperature variation along the water lines is less than 0.03°C for all operating temperatures in the range 3–50°C. The heat transfer coefficients between the circulating water, and both the guard and the cold plate, are measured to be approximately 5000 W m^{-2} K^{-1}. Negligible temperature differences therefore exist between the circulating water streams and the guard/cold plates.

The temperatures of the hot and cold water are measured with sensors inserted into re-entrant cavities at several points in each circulating water line. Measurements are made with two different types of sensors: mercury-in-glass bomb calorimeter thermometers (0.01°C resolution); and a Leeds and Northrup 8931 platinum resistance thermometer (nominally 100 Ω).

Whilst the compensating resistor in the bridge circuit effectively eliminates variations in the bridge output due to *long* term temperature fluctuations, *short* term fluctuations can cause large variations. These occur because the temperature of the metering piece responds only slowly to fluctuations in the guard temperature. This problem can be greatly reduced by sensing the guard temperature through a thermal low-pass filter. This consists of a thermal mass connected by a thermal resistance to the guard (see Fig. 2). The time constant of the low pass filter is designed to be the same as that for the metering piece. In the current apparatus, the thermal low pass filter reduces the magnitude of short term fluctuations ($\ll 1$ min) in the output of the thermistor bridge circuit by a factor of approximately five.

2.4. Measurement procedure

A critical step in setting up the apparatus is the identification of the null condition when the temperature of the metering piece is the same as that of the guard: $T_m = T_h$. This is particularly important with thermistor sensors since there is no well-defined zero in the relationship between the output of the bridge circuit and $T_h - T_m$. The null condition is established by supplying water of equal temperature to both sides of a highly insulating sample, and adjusting the output of the thermistor bridge circuit to zero.

It is necessary to be sure that the procedure for determination of the null condition does not alter any

heat flows from the metering piece, other than through the sample. One possible flow which could change during this procedure is along the glass plate on the hot side, through the bonded edge seal of the sample, to the cold side. The modelling results presented in Fig. 3 indicate that such heat flow should be negligible if the bonded edge is located outside the guard. An independent method of checking if the null condition is correct is also used: measurements are made of samples of very small, and calculable thermal conductance. The construction of such 'standard' samples is discussed in Section 2.6.

During the measurement of heat transport, the output of the thermistor bridge circuit is measured as a function of power to the metering piece, and the power at null is established by a best fit procedure. Care is taken to ensure that the system reaches steady state before recording data. The time constant for variations in bridge voltage is essentially determined by the thermal mass of the metering piece and the thermal impedance between the metering piece and guard. This time constant is calculated, and measured to be approximately 100 s.

2.5. Systematic errors in the apparatus

In Section 2.3, methods were described for reducing systematic errors in the apparatus due to parasitic heat flows from the metering piece to ambient. These heat flows can lead to time dependent and steady offsets in the null condition. There is a second source of systematic error in the apparatus which leads to inaccuracies in the apparent effective area of the measurement. These effects arise because of temperature differences within the guard and metering piece, associated with heat flow to the sample. This results in a difference in the null condition when heat is flowing through a sample, compared with the situation when no heat is flowing. This difference is proportional to heat flow and causes the measured heat flow to be consistently in error, by a constant proportion, compared with that calculated on the basis of the geometry of the apparatus.

The most obvious potential source of these temperature differences is due to the finite thermal impedance of the material of the metering piece and guard. It is readily shown, however, that this results in a small effect which can be made negligible by locating the temperature sensors for the guard and metering piece at approximately the same distance from the glass plate. (In the case of the guard, the point of connection of the low pass filter to the body of the guard determines the position at which the temperature is detected.) There is no practical advantage to be gained by using copper to fabricate the metering piece and guard rather than the brass which is currently used.

A much more serious source of temperature difference is associated with the layer of epoxy resin which is used to bond the metering piece and guard to the glass plate. A variation in the thickness of this layer

results in a temperature difference between the metering piece and guard which is proportional to the thickness difference and to the heat flow. The null condition during a heat flow measurement will therefore always be in error by an amount proportional to the heat flow. The apparatus behaves as if its effective area is different from that calculated from the geometry. For the apparatus with a 12 mm diameter metering piece and a 2 mm gap ($Z_{m-h} = 19 \text{ K W}^{-1}$), differences of 0.1 mm in the thicknesses of the layers of epoxy resin cause a change of ~12% in the effective area. The effective area increases if the epoxy resin is thicker in the guard region. The effect is exacerbated by the relatively low thermal conductivity of the epoxy resin (0.28 W m^{-1} K^{-1}).

A second mechanism exists through which variations in the thicknesses of the layers of epoxy resin cause a further apparent change in the effective area of the metering piece. If the layer of epoxy resin is thicker over the guard than over the metering piece, the front conducting surface of the metering piece is geometrically displaced towards the sample relative to the guard. This causes the heat flow from the metering piece to spread out radially further than would otherwise be expected. Finite element modelling indicates that a difference of 0.1 mm in the thicknesses of the epoxy resin layers causes an increase of ~6% in the heat flow from the metering piece due to this mechanism. The combined effect of these two mechanisms is additive.

Good absolute accuracy in the measurements of heat flow therefore requires variations in the thickness of the epoxy resin layer to be minimized. The thickness is measured during assembly of the apparatus and typically varies by less than 0.1 mm between the metering piece and guard regions, with the guard region being thicker. The effect of such variations could be reduced by loading the resin with thermally conductive powder. In this apparatus, when estimating the absolute value of heat flow, we apply a correction to the measurements based on the known thicknesses of the layers of epoxy resin.

In the above discussion, we have been concerned with temperature differences in the direction perpendicular to the plane of the sample. It has been implicitly assumed that temperature non-uniformities in the metering piece and the guard, parallel to the plane of the sample, can be neglected. Finite element modelling indicates that this is indeed the case. If the principles discussed here were applied to construction of an apparatus with a much larger measurement area, however, the effects of lateral temperature differences would need to be examined quite closely.

2.6. Design of standard samples

It is highly desirable to check the performance of the equipment by measuring samples of known thermal conductance. In order to do this, several 'standard' samples were manufactured which either have a known thermal conductance or for which the thermal

conductance of a particular sample is calculable in terms of the conductance of other samples. Figure 4 shows a schematic diagram of a standard sample. Two plane sheets of glass are held in a 'clamped edge' configuration and sealed with Viton O-rings to stainless steel flanges. The separation of the glass sheets is maintained by two rings of pillars which are remote from the central region through which heat flow is to be measured. Finite element modelling is used to demonstrate that the heat flow due to the pillars is negligible in the central region (see Section 3.4).

Heat flow due to conduction through gas at low pressure is given by [3, 9]:

$$Q_{gas} \approx 0.375 pA(T_1 - T_2), \qquad (2)$$

where p is the pressure in Pa. Since the standard samples are continuously evacuated to a pressure $< 10^{-3}$ Pa, gas conduction is negligible. Both conventional diffusion pumps, and appendage ion pumps are used for this purpose.

Heat flow through these standard samples is therefore by radiation only. The amount of radiative heat flow between plane, parallel surfaces of area A at temperatures T_1 and T_2 can be calculated from the angular dependent emittances of the surfaces $\varepsilon_1(\theta)$ and $\varepsilon_2(\theta)$:

$$Q_{radiation} = \varepsilon_{combined}\sigma A(T_1^4 - T_2^4), \qquad (3)$$

where σ is the Stefan–Boltzmann constant. $\varepsilon_{combined}$ is called the combined emittance of the two surfaces and is written [10]

$$\varepsilon_{combined} = \int_0^{\pi/2} \left(\frac{1}{\varepsilon_1(\theta)} + \frac{1}{\varepsilon_2(\theta)} - 1 \right)^{-1} \sin 2\theta \, d\theta. \qquad (4)$$

These equations are derived on the assumption that radiation which is not absorbed by either surface is reflected specularly.

The evaluation of $\varepsilon_{combined}$ requires a knowledge of the angular dependence of emittance of each surface. The angular dependence can be measured directly, or obtained from optical measurements of the refractive index through the Fresnel formula [10]. Geotti-Bianchini and Lohrengel [10] also describe a methodology for calculating the combined emittance in terms

of an 'effective emittance' ε' of each surface, and using the simpler relationship

$$\varepsilon_{combined} = (\varepsilon_1^{-1} + \varepsilon_2^{-1} - 1)^{-1}. \qquad (5)$$

For uncoated soda-lime glass, Geotti-Bianchini and Lohrengel measured $\varepsilon' = 0.839$, in close agreement with the value of 0.845 proposed by the ISO standard [11]. These values of ε' give $\varepsilon_{combined}$ for two uncoated glass surfaces which differ by $\sim 1\%$, and which are also very close to the value which would be obtained by simple application of equation (5) using the accepted value of 0.837 for the hemispherical emittance of glass [12]. We emphasize, however, that the close coincidence between estimates of radiative heat flow for two glass surfaces using values for hemispherical and effective emittance in equation (5) does not occur for conducting surfaces. In the latter case, the increase in emittance for radiation at large angles to the normal makes it essential to use values of effective emittance in equation (5), or to carry out the full integration in equation (4).

The separation of the inner surfaces in the standard samples is determined principally by the height of the support pillars and is approximately 0.2 mm. This is sufficiently large to ensure that direct evanescent field radiative coupling between the inner surfaces of the samples [13] is negligible and that there is negligible difference in the level of vacuum in the region between the plates compared with that in the surrounding region. The surfaces are sufficiently close together, however, that negligible radiative loss occurs through the outer gap between them.

3. RESULTS

In this section, we present the results of measurements made with the apparatus which indicate the reproducibility and accuracy that has been achieved. We also show how the contributions to heat flow through a sample due to different physical effects can be identified separately.

3.1. Measurement of thermal conductance

Figure 5 shows measurements of the bridge voltage (at the output of the amplifier) as a function of power dissipated in the metering piece for several different samples. A linear relationship exists for all samples. The thermal impedance between the metering piece and guard, Z_{m-h}, can be calculated from the slope of these lines, the gain of the amplifier (which depends on the actual value of the resistance of the thermistors at the operating temperature) and the temperature dependence of resistance of the thermistors. As noted in Section 2.3, we find that $Z_{m-h} = 19$ K W^{-1}, which is reasonably consistent with the modelling result.

As discussed above, in precise measurements it is important that a good thermal contact exists between the apparatus and the sample. If the contact gel does not completely fill the gap between these two components, the additional thermal impedance of the air
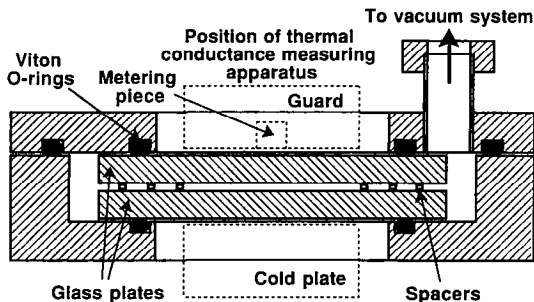

FIG. 4. Schematic diagram of a standard sample. The dashed lines show the operating position of the measurement apparatus.
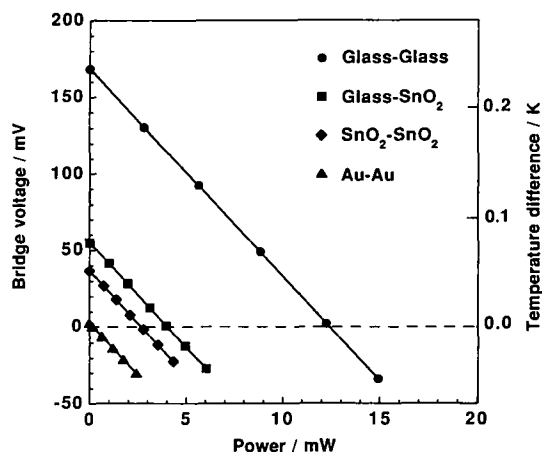
FIG. 5. Amplified output of the bridge circuit as a function of power dissipated in the metering piece, for several samples. A scale which indicates the magnitude of the temperature difference between the metering piece and guard is also shown. The temperatures on the outer surfaces of the hot and cold glass plates are approximately 23 and 3°C respectively.

layer decreases the heat flow through the sample, and lateral heat flow along the glass plates is larger. A measurable increase also occurs in Z_{m-h} and this is evidenced by a change in the slope of the bridge voltage as a function of power to the metering piece. In all precise measurements, the slope of this straight line is routinely monitored and is found to be constant to within 0.2% for repetitive measurements at a specific position on an individual sample.

3.2. Accuracy of the apparatus

It is important to be able to relate the small area measurements of heat flow obtained in this apparatus with the determination of large area heat flow through practical evacuated windows. In order to do this, it is necessary that an estimate be made of the absolute accuracy of the experimental results. This firstly requires that the magnitude of parasitic heat flow from the metering piece be determined—essentially this involves setting a limit on the accuracy with which the zero of the apparatus is known. Secondly, the apparatus should be calibrated by measuring the magnitude of heat flow through a sample of known thermal conductance—in essence, this is equivalent to measuring the effective area of the apparatus.

Limits to the magnitude of parasitic heat flow from the metering piece have been set by measuring a dynamically pumped standard sample with two internal gold surfaces. The gold films are ~ 300 nm thick, and were deposited by vacuum evaporation. The hemispherical emittance of the gold films, as determined from optical measurements, is 0.015 ± 0.002. The measured heat flow through this sample is 0.150 mW for the hot and cold surfaces at approximately 23 and 3°C respectively. On the assumption of an effective area of 1.69 cm^2 (see below), this corresponds to an emittance of 0.017, calculated from equations (3) and (5). The equivalent thermal conductance of

such a sample is 0.050 W m^{-2} K^{-1}. Measurements of heat flow through this sample at other temperatures (45°C/20°C for T_h/T_c) yield an identical value for the emittance of the gold films. We conclude that parasitic heat flows from the metering piece are smaller than an equivalent thermal conductance of 0.01 W m^{-2} K^{-1}. (In the preceding discussion, we ignore the difference between hemispherical emittance and effective emittance. The error arising from this is smaller than that in the experimental measurements for these very low emittance surfaces.)

The effective area of the apparatus can be estimated using measured values of heat flow for dynamically pumped standard samples with uncoated glass surfaces, and using an effective emittance of 0.839 in equation (5). The effective area as determined in this way is 1.69 cm^2, corresponding to a circle of radius 7.33 mm.

Confirmation of this estimate of effective area can be obtained by measurements on a calibration sample of known thermal conductance, and by numerical modelling. The calibration sample used in this work is a 25.3 mm thick, 130 mm diameter disk of NBS fibrous glass board standard reference material SRM1450a [14]. Values of thermal resistance of this material are quoted to an accuracy of $\pm 2\%$. The material is compressed between two glass plates to a thickness of 25.0 mm. The total thickness of the glass on each side of the reference material is 6 mm, which is identical to that for measurements on evacuated window samples. Measurements on this reference material yield a value for the effective area of the metering piece of 1.64 cm^2, corresponding to a circle of radius 7.23 mm.

The effective area of the apparatus can also be estimated by numerical modelling, provided that the effects of thickness variations in the epoxy resin bonding layer are included. Within experimental uncertainties, measurements on the dynamically pumped standard uncoated glass sample and on the standard reference material give mutually self-consistent estimates of the effective area of the apparatus with those obtained by such modelling. We therefore conclude that the accuracy of the heat flow measurements made with this apparatus is at least as good as that of the calibration sample ($\pm 2\%$), and possibly somewhat better. In the results quoted here, we use the value of effective area obtained from measurements on standard samples with uncoated glass inner surfaces.

Measurements were made on dynamically pumped standard samples in which the internal surfaces were systematically changed. The results of these measurements confirm that direct application of the simple expression for combined emittance of two surfaces (equation (5)) does not accurately estimate the radiative heat flow between conducting surfaces when the angular dependence of emittance is ignored. For example, equation (5) was used to determine a value for the emittance of SnO$_2$ coated glass by comparing data from two symmetric samples with (a) two

uncoated glass inner surfaces and (b) two SnO₂ coated glass inner surfaces. The emittance of the SnO₂ coated glass so obtained was 0.23. This value was used in equation (5) to estimate the radiative heat flow in an asymmetric sample with one uncoated glass inner surface and one SnO₂ coated glass inner surface. This estimate was approximately 6% higher than the measured heat flow in such a sample. We attribute this discrepancy to the different angular dependencies of the emittance of the insulating and conducting surfaces [10]. Such effects are being studied in more detail.

3.3. Reproducibility of heat flow measurements

An important goal of this work is to achieve a high level of reproducibility for sequential measurements on an individual sample. This is an essential requirement for a life-test program. Figure 6 shows examples of measurements on several samples, made over a period of many weeks. Variations in the measured value of thermal conductance are less than ± 0.004 W m^{-2} K^{-1} except for one sample with glass internal surfaces. This sample exhibits slightly higher heat transfer than normal, which we believe is due to direct evanescent field radiative coupling [13] between the internal surfaces. These surfaces are separated by approximately 30 μm in this sample, somewhat less than 100 μm typical of the other samples. We attribute the variations in total heat flow to slight changes in this small separation. On the basis of these measurements, it is concluded that the reproducibility of the apparatus is better than ± 0.004 W m^{-2} K^{-1}.

3.4. Heat flow through the pillars

The small size of the measuring area of the apparatus permits the heat flow through the support pillars to be identified separately from that due to radia-

FIG. 7. Heat flow due to a single small support pillar through a circular measuring area. The results are presented in dimensionless form in terms of the total heat flow through the pillar, Q_{total}, and the total thickness, t, of the glass on the measurement side of the sample.

tion and conduction through residual gas. The temperature gradient in the glass plate at the outer isothermal surface of the glass due to heat flow through a single support pillar was determined by numerical modelling. These data can be used to calculate the heat flow due to a single pillar which is detected by a circular measuring area as a function of axial separation of the pillar and the measuring area. Figure 7 shows the results of such a calculation. The data of Fig. 7 are presented in dimensionless form in terms of the total calculated heat flow through the pillar, Q_{total}, and the total thickness, t, of the glass plates (sample plus apparatus) on the side of the metering piece and guard.

Figure 8 shows measured, and calculated values of heat flow through a 14 mm diameter area, due to radiation and pillar conduction, along the diagonal of a unit cell of a square array of metal pillars,
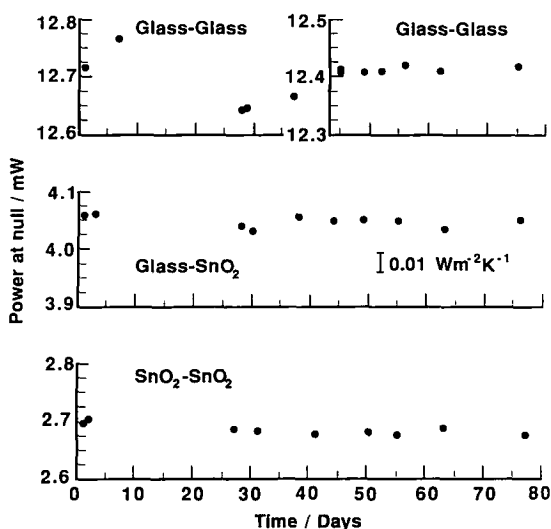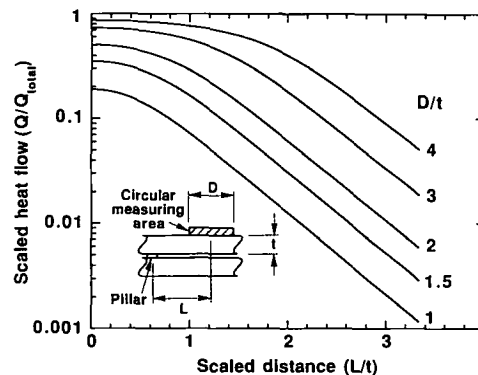

FIG. 6. Measurements of power to the metering piece, at null, for several samples over an extended period. The power axes are offset from zero, but have the same scale.
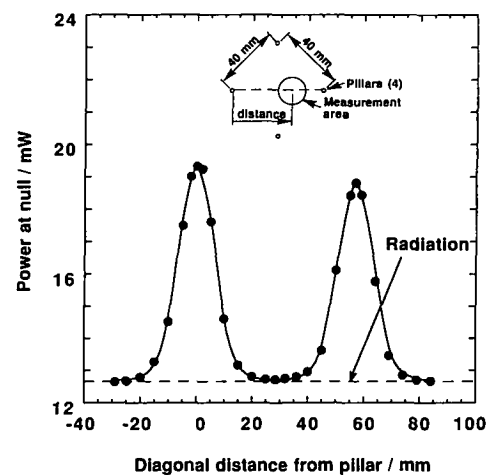

FIG. 8. Measured (points) and calculated (solid line) values of heat flow through a circular area along the diagonal of a unit cell of a square pillar array. The sample is sealed, and the inner glass surfaces are uncoated. The metal pillars are approximately 0.6 mm in diameter and are separated by 40 mm.
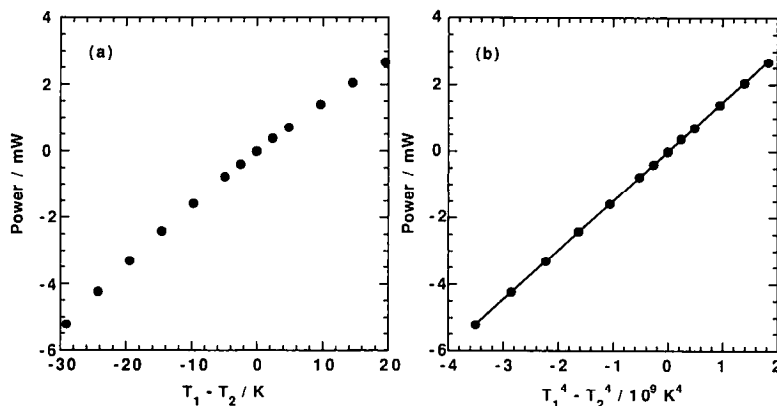
FIG. 9. (a) Measured heat flow as a function of the temperature difference between the inner surfaces of a sample, $T_1 - T_2$. In these measurements, the temperature of the hot bath is maintained constant at 23 C. This sample has SnO_2 coatings on both inner surfaces. (b) The data of (a) replotted as a function of $T_1^4 - T_2^4$. The linear dependence indicates that the heat flow is predominantly radiative.

approximately 0.6 mm in diameter and separated by 40 mm. In these data, the total glass thickness is 6 mm (4 mm in the sample and 2 mm in the apparatus), the inner surfaces of the glass sheets are uncoated, and gas conduction is negligible. The temperatures of the guard and cold side are approximately 23 and 3°C respectively. The calculated heat flow is normalized to the measured heat flow at the position of each pillar, and at the midpoint of the pillars. The experimental and numerical results are in excellent agreement.

The data of Fig. 8 show that heat flow due to pillars in the middle of the unit cell of the pillar array is small, but measurable. This heat flow becomes relatively more important when samples with very low emissivity internal coatings are measured. For example, the pillars contribute approximately 1% of total heat flow in the centre of a square array of 0.6 mm diameter pillars, separated by 40 mm, for a sample with two internal surfaces each of emittance 0.2. We conclude that to achieve high accuracy and reproducibility, it is necessary to consider carefully the contribution from the pillars at all points within the sample.

3.5. *Estimate of heat flow by gas conduction*

Figure 9(a) shows measurements of the heat flow through a sealed sample as a function of temperature difference between the inner surfaces of the sample. The temperatures of the inner surfaces, T_1 and T_2, are determined from the measured temperature of the hot and cold baths and the calculated temperature difference across the glass plates on each side. The temperature of the hot bath is constant at 23°C in these measurements. This sample is permanently sealed, with SnO_2 coatings on both inner surfaces. The non-linear dependence of heat flow on temperature difference is clearly evident. The data of Fig. 9(a) are replotted in Fig. 9(b) as a function of $T_1^4 - T_2^4$. A linear relationship is obtained indicating that the heat flow is predominantly radiative. Curve fitting tech-

niques can be used to show that the linear component of heat flow (i.e. proportional to $T_1 - T_2$) is less than 0.02 W m^{-2} K^{-1} for these data. Such a linear dependence could be due to pillar, or gas conduction. In this sample, modelling shows that pillar conduction contributes less than 0.01 W m^{-2} K^{-1} to the total measured conductance. We can therefore use equation (2) to infer that the gas pressure within this sample is less than about 0.03 Pa.

4. CONCLUSION

An apparatus has been constructed for measuring the local heat transport in samples of flat evacuated glazing. Accurate estimates of the separate contributions to heat flow through the sample from pillar conduction, conduction through residual gas and thermal radiation have been obtained. The magnitude of parasitic heat flow in the apparatus is less than an equivalent thermal conductance of 0.01 W m^{-2} K^{-1}. The effective area of the apparatus, as determined by numerical modelling, agrees with that obtained from measurements on a thermal calibration standard, and with published values for the emittance of glass. The accuracy of the apparatus is better than $\pm 2\%$. The reproducibility of repetitive measurements over a period of approximately 80 days is equivalent to a conductance variation of ± 0.004 W m^{-2} K^{-1}.

REFERENCES

1. Sir James Dewar, *Collected papers of Sir James Dewar* (Edited by Lady Dewar). Cambridge University Press, Cambridge (1927).
2. A. Zoller, Hohle glasscheibe, Deutsches Reich Patentschrift Nr. 387655 (1913).
3. R. E. Collins and S. J. Robinson, Evacuated glazing, *Solar Energy* **47**, 27–38 (1991).
4. R. E. Collins, A. C. Fischer-Cripps and J.-Z. Tang, *Solar Energy* **49**, 333–350 (1992).
5. R. E. Collins, L. Poladian, B. A. Pailthorpe and R. C. McPhedran, Heat conduction through support pillars in evacuated windows, *Aust. J. Phys.* **44**, 73–86 (1991).
6. R. E. Collins and A. C. Fischer-Cripps, Design of pillar arrays in flat evacuated windows, *Aust. J. Phys.* **44**, 545–564 (1991).
7. AS1288, Glass in buildings—selection and installation, *Australian Standards Association* (1989).
8. K. G. T. Hollands, Natural convection in a horizontal layer of air with internal constraints, Ph.D. Thesis, McGill University, Montreal, Canada (1967).
9. R. J. Corrucini, Gaseous heat conduction at low pressures and temperatures, *Vacuum* **7–8**, 19–29 (1957).
10. F. Geotti-Bianchini and J. Lohrengel, Measured angular distribution of the emissivity and calculated radiation heat transfer of architectural coated flat glass, *Glastech. Ber.* **62**, 312–357 (1989).
11. ISO TC 160/SC2/WG2, Thermal insulation of glazing. Calculation rules for determining the steady state U value (thermal transmittance) of double or multiple glazing, *International Standards on the thermal and radiometric properties of glazing*, GEPVP, Brussels (1986).
12. M. Rubin, Optical properties of soda-lime silicate glasses, *Solar Energy Mass.* **12**, 275–288 (1985).
13. D. Polder and M. van Hove, Theory of radiative heat transfer between closely spaced bodies, *Phys. Rev. B* **4**, 3303–3314 (1971).
14. M. C. I. Siu, Fibrous glass board as a standard reference material for thermal resistance measurement systems. In *Thermal Insulation Performance*, ASTM STP 718 (Edited by D. L. McElroy and R. P. Tye), 343–360, American Society for Testing and Materials (1980).